

We are IntechOpen, the world's leading publisher of Open Access books Built by scientists, for scientists

4,800

Open access books available

122,000

International authors and editors

135M

Downloads

Our authors are among the

154

Countries delivered to

TOP 1%

most cited scientists

12.2%

Contributors from top 500 universities



WEB OF SCIENCE™

Selection of our books indexed in the Book Citation Index
in Web of Science™ Core Collection (BKCI)

Interested in publishing with us?
Contact book.department@intechopen.com

Numbers displayed above are based on latest data collected.

For more information visit www.intechopen.com



Application of Holograms in WDM Components for Optical Fiber Systems

Alfredo Martín Mínguez and Paloma R. Horche
*ETSIT-Universidad Politécnica de Madrid
Spain*

1. Introduction

Coarse Wavelength Division Multiplexing (CWDM) technologies are being widely deployed internationally in metropolitan and access networks due to the increased demand for delivering more bandwidth to the subscriber, created by the need of enhanced services, (Koonen, 2006). For metro, and mainly for access networks applications, an increment in capacity may be achieved with a cost-effective multiplexing technology without the need for the high channel counts and closely spaced wavelengths typically used in long haul networks. A channel space of 20 nm, as proposed in the G. 694.2 ITU Rec., can be used relaxing the processing tolerances and potentially lowering the cost of components. CWDM technology reaches those requirements and it has been proposed for these applications. It is in this context that holographic optical devices have a potential use.

This chapter describes the theory, design, and experimental results of a generic multipurpose device that can operate as a tunable wavelength filter, wavelength multiplexer and wavelength router. This device could be especially useful in optical network applications based on both Coarse and Dense Wavelength Division Multiplexing technology (CWDM/DWDM). The enabling component is a Ferro-electric Liquid Crystal (FLC) Spatial Light Modulator (SLM) in which dynamic holograms are implemented in real time. As a consequence, the device will be able to carry out different functions according to the hologram recorded on the SLM. The great advantage of this device is polarization insensitivity in the region of operation, allowing low cross-talk and simple handling. As hologram management is the basis for this device, some topics in the Computer Generated Hologram (CGH) design process are commented on and general guidelines are also considered.

Laboratory experiments have demonstrated the capability of a phase FLC-SLM, with the great advantage of polarization insensitivity operation, to diffract the incident light according its wavelength and hologram patterns, for the use in the former applications.

Two typical applications of this technology are described: the first one is a design of an equalized holographic Reconfigurable Optical Add-Drop Multiplexer (ROADM), where this device can address several wavelengths at the input to different output fibers, according to the holograms stored in a SLM (Spatial Light Modulator), all the outputs being equalized in power; the second one is dealing with the design of an holographic router with loss compensation and wavelength conversion whose main application is in Metro networks in the interconnection nodes. This device uses a SOA (Semiconductor Optical Amplifier), in the non linear region, to do the wavelength conversion and, in addition, to supply the gain in order to compensate for the intrinsic losses of the holographic device.

2. Operating principle

The working principle of a holographic device design is based on the wavelength dispersion produced in a diffraction grating element (Agrawal, 2002). When a polychromatic light reaches a diffraction grating, there is an angular dispersion (diffraction) according to the incident light wavelength.

Equation (1) expresses the relationship between the diffraction angle and the wavelength of the incident light λ :

$$\sin \Phi = \frac{m\lambda}{d} \quad (1)$$

by considering the incident light perpendicular to the grating, Φ is the diffracted light angle, m is the diffraction order and d the grating spatial period.

The light diffracted, in a far field approximation, follows the Fourier transform distribution and the intensity for the different diffraction orders, m , is proportional to $\text{sinc}^2(\Phi d/\lambda)$; the separation between diffraction orders is given by $\lambda R/d$, where R is the distance between the binary transmissive diffraction grating and the Fourier plane (Kashnow, 1973).

Most diffraction grating elements are not practically useful for changing the spatial period or the wavelength. A way to allow these variations is, by using a Spatial Light Modulator (SLM), to implement on it a Computer Generated Hologram (CGH). The pixelated structure of the SLM produces the effect of a two-dimensional diffraction grating when the device is illuminated with a coherent light. In the SLM every ferro-electric liquid crystal (FLC) pixel can be electro-optically configured to provide a phase modulation to the incident light. Therefore, by managing the hologram on the SLM and its spatial period a programmable diffraction grating is obtained.

In optical fiber communications, wavelengths around 0.8 – 1.6 μm are used. Thus, an SLM pixel pitch close to these wavelength values is required. Unfortunately, current commercial SLMs do not have enough resolution. Therefore, to solve this limitation, a fixed diffraction grating with a low spatial period, together with the SLM giving a high resolution filter, is used (Parker et al., 1998).

	2-Phases		4-Phases	
	% darkness	PHASE (rad)	% darkness	PHASE (rad)
black	100	0	100	$\pi/4$
grey1	-	-	66	$3\pi/4$
grey2	-	-	33	$-3\pi/4$
white	0	π	0	$-\pi/4$

Table 1. Relationship between phases and contrast

2.1 2 and 4-phases holograms

Different types of holograms can be used (Horche & Alarcón, 2004) in the SLM. In order to optimize losses, phase holograms are preferred instead of amplitude holograms due to its intrinsic 3 dB of loss and 4-phase holograms are used instead of 2-phase (binary) holograms because of its greater efficiency (40.5% \rightarrow 81%), which is proportional to $\text{sinc}^2(\pi/M)$, where M is the number of phases. Table 1 summarizes the relationships between phase and contrast for 2 and 4 phase holograms.

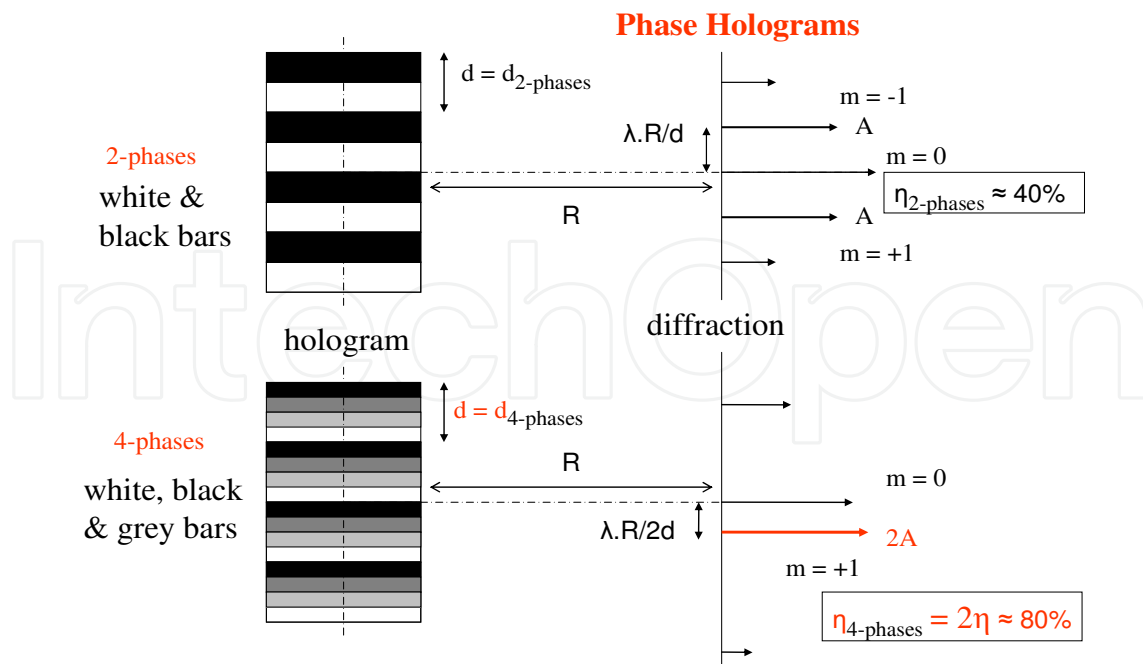


Fig. 1. two/four-phases bars holograms

Fig 1 shows a bars hologram for 2 and 4-phases and their diffraction target in a far field approach. As we can see, the main difference in the holograms is the grey bars in the 4-phases holograms; in this case there is a white bar, a black bar and two different grey bars for addressing the 4-phases ($\pi/4, 3\pi/4, -3\pi/4, -\pi/4$); with regard to the diffraction target. Another characteristic is the loss of the symmetry for the diffraction orders.

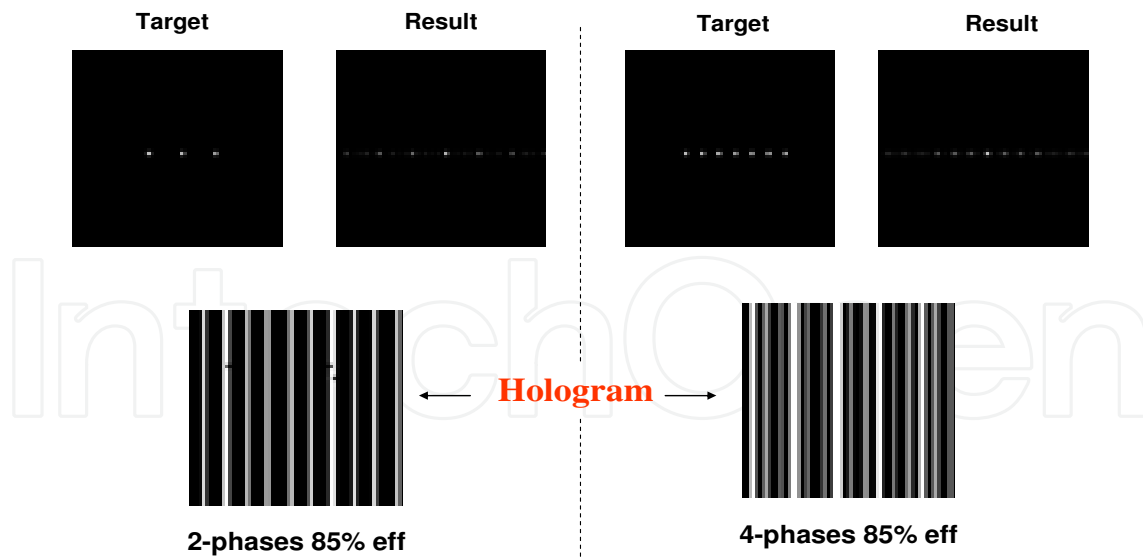


Fig. 2. Examples of 2/4-phases holograms and diffraction targets

In Fig. 2 examples of calculated holograms are shown. The program calculates the inverse Fourier transform (F.T.)⁻¹ of the diffraction target (result) by an annealing optimization algorithm. In this case both holograms have a calculated efficiency of 85% and the grey bars are clearly visible in the figure. In the following Section some guidelines about design of holograms by computer are given.

2.2 Computer generated hologram design

Taking into account the former considerations and by implementing a hologram on the SLM where its spatial period can be modified in real time, we obtain a programmable diffraction grating.

The relationship between the hologram and its Fourier Transform function are:

Hologram → F.T. → Diffraction target

Diffraction target → F.T.⁻¹ → Hologram

In order to implement the CGH, holograms are calculated by using a program based on a variation of the widely adopted simulated annealing optimization algorithm (Dames, Dowling et al., 1991), (Broomfield, Neil et al., 1992) whose cost function to minimize the calculation error is:

$$C = \sum_t \frac{(I_i^2 - A^2)^2}{A_i^2} \quad (2)$$

where I_i^2 is the calculated spot intensity for the diffraction order i ; A_i^2 is its defined intensity and A^2 is the average intensity for the diffraction target spots; t is the number of process calculations.

There are three steps in a CGH design process:

1. Target definition: the target is the diffraction pattern that is to be obtained from the SLM. Depending on the use: filter, switch or others, this target is usually an array or a matrix of spots. This is the input for the program.
2. Fourier transform calculation: the program calculates the inverse Fourier transform (F.T.)⁻¹ of the target. The optimization algorithm compares the FT of the hologram with the defined target improving the efficiency at each calculation time. Hologram pixels are flipped between the amplitude values 0, 1 (or phase 0, π) to reduce an error function, (2), specifying the difference between the desired target in the Fourier plane and the reconstruction obtained from the current state of the hologram, improving the efficiency at each calculation (Efficiency defined as: $\eta = \Sigma m \text{ orders diffracted light} / \text{total incident light}$).
3. Finally, CGH implementation in an optical substrate, using a photographic film or SLM.

The CGH designed for this work is a black & white bars pattern implemented onto a Spatial Light Modulator, where there are only two possible states: "1" for white (total transparency or π phase shift) and "0" for black (total darkness or 0 phase shift). Fig. 3 shows the original diffraction target (a), an array of spots with different light intensities (non uniform, as in Fig. 3a), and three consecutive holograms (b, c, d), calculated by the program carrying out the inverse FT according to the algorithm efficiency. A 45% efficiency is an initial calculation value and close to 90% efficiency is practically the best result in the optimization process.

During the calculation of the hologram, the program can find out different holograms which match the diffraction target. It is possible to change, dynamically, the initial conditions (original diffraction target and efficiency, optimization process parameters), to change the direction for the optimization process allowing the algorithm to escape from local minima and reach the correct hologram.

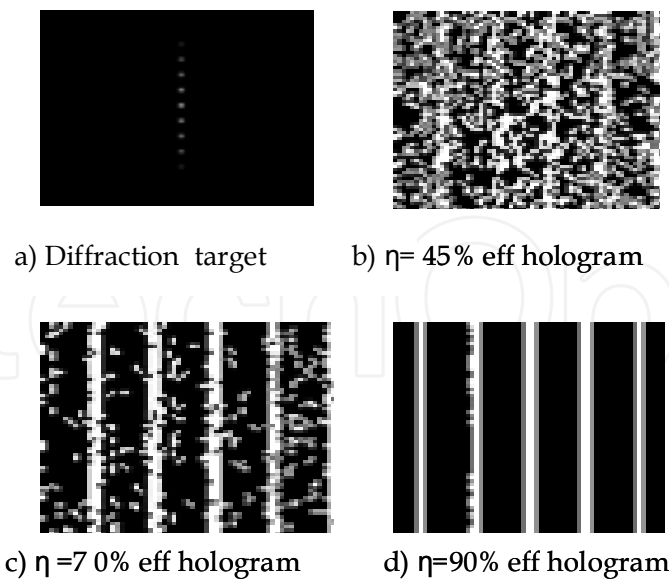


Fig. 3. Hologram calculation process according to the algorithm efficiency η . a) diffraction target; b), c) and d) are calculated holograms with $\eta = 45\%$, 70% and 90% , respectively

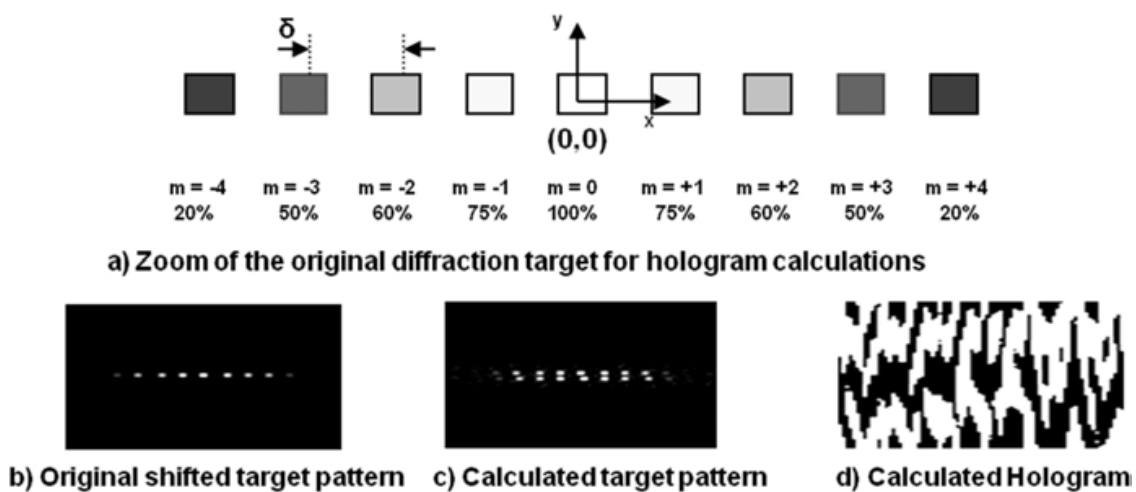


Fig. 4. a) "Zoom" of the original diffraction target, b) original shifted diffraction pattern along the y axis, c) calculated diffraction target and d) corresponding hologram when the original pattern is shifted

Computer calculations are very sensitive to the geometrical distribution of the original diffraction target. A very slight misalignment on it (centre: $x = 0$, $y = 0$) can produce a hologram completely different from the correct one. This effect is shown in Fig. 4 when the original array of spots (Fig. 4a) is shifted by 30% of spot separation δ (Fig. 4b), along the vertical axis y ; the calculated target (Fig. 4c) is an array of spots "duplicated" and "shifted" instead of a singular one.

To avoid small misalignments, along the x axis, of the output fibers array positions, with impact on the efficiency, we can optimize the hologram pattern, introducing an offset in the bar positions to correct them (Crossland et al., 2000) An offset of 5% of the hologram period would impact the efficiency up to a 40%.

For the operation of holographic devices after the generation of holograms, it is necessary to configure with them the SLM. To perform the switching operation a closed control between the holographic component (SLM) and the computer is needed to assign the correspondent hologram from a local database. This procedure is represented in Fig. 5, where a switching control acts over the PC-SLMs interface.

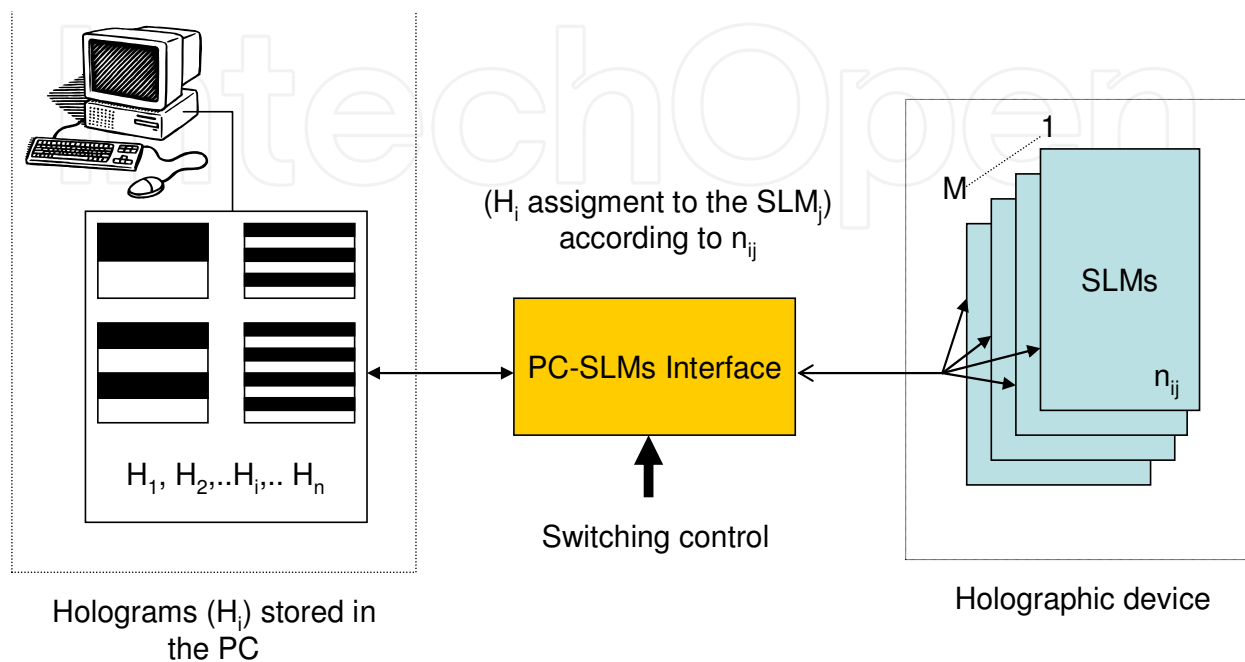


Fig. 5. Tunable holographic device: switching operation

3. Dynamic holographic device design

In order to design a holographic optical device a “4f” structure is chosen using a transmissive SLM and fixed grating. Fig. 6 illustrates the device used in the present work. The previously calculated CGH (black and white bars) is loaded onto the SLM via a PC-based interface. The SLM-FLC and fixed grating are illuminated by light coming from a singlemode optical fiber collimated by means of a lens. A second lens produces the replicated array of spots explained above on the back focal plane of the lens.

In our experiments, we are interested only in the array of spots corresponding to the first order of diffraction. Therefore, the output optical fibers array is placed in the back focal plane of the lens at a certain angle in order to optimize the coupling. Because of the small size of the singlemode fiber radius, it acts as a spatial light filter.

Output fibers F_1, \dots, F_{10} , must be located at the Fourier lens plane in order to receive the maximum light intensity of the diffracted beams. The relationship between the system diffraction angles (Parker et al., 1998) is in agreement with the expression:

$$\arctan\left(\frac{x}{f}\right) = \arcsin\left(\frac{\lambda}{d}\right) + \arcsin\left(\frac{\lambda}{H}\right) \quad (3)$$

where x is the distance of the output optical fiber from the optical axis, f is the focal length of the lens, d is the spatial period of the fixed grating and H is the hologram spatial period,

which relationship with D , the size of the pixel, and N , the number of pixels in one dimension of the SLM is given in (4):

$$H = \frac{ND}{n} \quad 0 < n < \frac{N}{2} \quad (4)$$

where n is the integer number of black & white bar pairs and depends on the type of hologram (pattern). For small angles, equation (3) can be simplified as follows:

$$\lambda \approx \frac{x}{f} \cdot \frac{1}{\left(\frac{n}{ND} + \frac{1}{d}\right)} \quad (5)$$

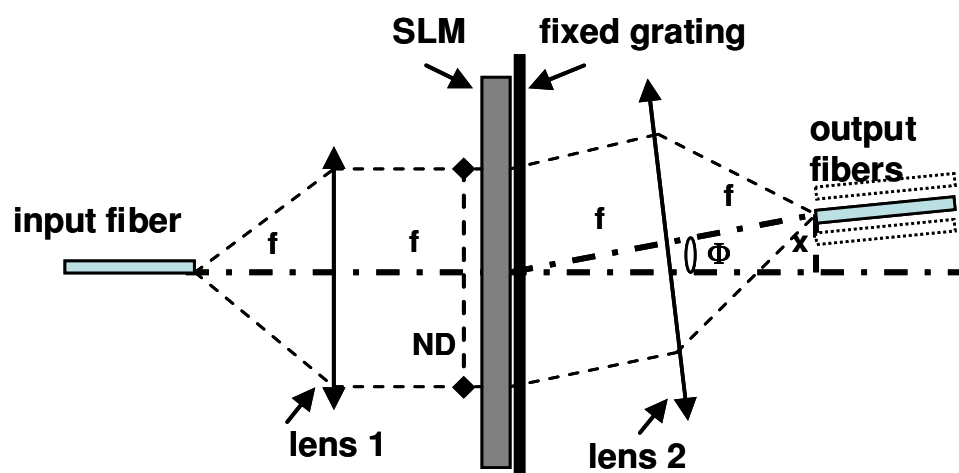


Fig. 6. "4f" dynamic holographic device with a transmissive SLM and fixed grating.

When the other holographic device parameters are fixed, λ only depends on n , as can be shown from (5). According to fixed or variable values for n or/and x , different applications for our device can be considered giving an idea of the device's versatility (see Table 2).

In the following sections, we design a generic multipurpose device based on the experimental scheme explained above that can operate as a tunable wavelength filter, wavelength multiplexer and wavelength router, by simply modifying in real time the CGH loaded on the SLM. The PC-based interface used to load the CGH on to the SLM also serves to calculate the different patterns needed. The electronic interface allows an automatic program to be developed for loading different patterns when they are needed.

n	x	Application
fix	fix	Holographic band-pass filter
variable	fix	Tunable holographic band-pass filter
fix	variable	Demultiplexer 1x M
variable	variable	λ router 1x M

Table 2. Different device applications

In all cases, the central wavelength channel, λ_0 , is obtained for $n = N/4$ in (5), and the operating wavelength range $\Delta\lambda_f$ is given by:

$$\Delta\lambda_f = \lambda(n=0) - \lambda\left(n = \frac{N}{2}\right) \quad (6)$$

The -3dB passband width, BW , for each wavelength channel tuned, is limited by the output fiber characteristics and the wavelengths coupled inside the core diameter ϕ_{core} . Taking this into account, and from (3), the following expression relates the bandwidth BW for every wavelength channel tuned in the filter and the focal distance f of the lens according to the optical power coupled into the output optical fiber (Parker et al., 1998):

$$f > \phi_{core} \frac{d}{BW} \times \left(1 - \frac{\lambda_0^2}{d^2}\right)^{3/2} \quad (7)$$

In order to obtain minimum losses, the collimated light through the SLM has to illuminate the maximum quantity of pixels. As its intensity distribution has a Gaussian profile, it is sufficient that $1/e^2$ beam bandwidth illuminates the SLM aperture. According to optical Gaussian laws, the following condition is reached:

$$ND = 4\lambda_0 \frac{f}{\pi\phi_{core}} \quad (8)$$

For commercial FLC-SLMs, available pixel size D is $> 5 \mu\text{m}$ and the number of pixels, N , usually is from 250 to 1000. From expressions (5) and (7), it is possible to calculate the x value and λ_{max} and λ_{min} for the operating range of tuning.

4. Tunable holographic filter application

In order to design a tunable holographic filter with a -3dB passband width, BW , of 1 nm (125 GHz), for each wavelength channel tuned, we take $d = 3.5 \mu\text{m}$ for the spatial period of the fixed grating. To use the same device for CWDM/DWDM, a SLM with a value of $N = 720$ and $D = 7 \mu\text{m}$ for the spatial period, is chosen. The output singlemode fibers used in our device have a core diameter, ϕ_{core} , of $9 \mu\text{m}$. Then, from (7), f must be greater than 23.9 mm. As a practical value we assume $f = 25 \text{ mm}$.

Table 3 summarizes the filter figures for CWDM systems applications where channels are allocated between $\lambda_{min} = 1290 \text{ nm}$ and $\lambda_{max} = 1590 \text{ nm}$, with central wavelength $\lambda_0 = 1431 \text{ nm}$, and for DWDM systems ($\lambda_{min} = 1530 \text{ nm}$ and $\lambda_{max} = 1590 \text{ nm}$, $\lambda_0 = 1551 \text{ nm}$).

CWDM		DWDM
1270 -1590	$\Delta\lambda$ (nm)	1510 -1590
1	BW (nm)	1
1431	λ_0 (nm)	1551
25.00	f (mm)	25.00
11.499	x (mm)	12.463
24.71	Φ (°)	26.51
1591	λ_{max} (nm)	1591
1311	λ_{min} (nm)	1531

Table 3. Device parameters for CWDM(DWDM) systems

The operation as a tunable CWDM/DWDM filter is obtained by changing the hologram period, n . From the output fibers (F_1 to F_{10}), a CWDM tunable filter uses F_4 and a DWDM tunable filter uses F_8 (see Fig. 6).

In Table 4 tuning between $1311 < \lambda < 1591$ nm (CWDM, output fiber F_4) is obtained for $17 < n < 328$ and between $1531 < \lambda < 1591$ nm (DWDM, output fiber F_8) is reached for $138 < n < 201$.

a)	n	328	276	227	180	136	94	55	17
	λ (nm)	1311	1351	1391	1431	1471	1511	1551	1591
b)	n	201	180	159	138				
	λ (nm)	1531	1551	1571	1591				

Table 4. a) Filter operation for CWDM (F_4) and b) for DWDM (F_8)

4.1 Wavelength response

For CWDM applications the holographic filter has a tuning range of $\Delta\lambda_f = 1591 - 1311 = 280$ nm with a -3dB passband of 1 nm. In Fig. 7 the transmission response is shown, according to (Parker et al., 1998). For wavelengths very close to the centre, the shape is Gaussian ($\lambda < \lambda_0 \pm 1.5$ nm); from these wavelengths the shape is like a Bessel function and the zero convergence is slower (> 20 dB for $\lambda > \lambda_0 \pm 1.5$ nm ; > 40 dB for $\lambda > \lambda_0 \pm 5$ nm).

Table 5 shows, in case of CWDM systems, the different values of n and corresponding central wavelengths separated by 40 nm, from 1311 to 1591 nm. In this case, an adjacent channel isolation > 50 dB is achieved and the complete filter tuning range is covered according to the type of hologram.

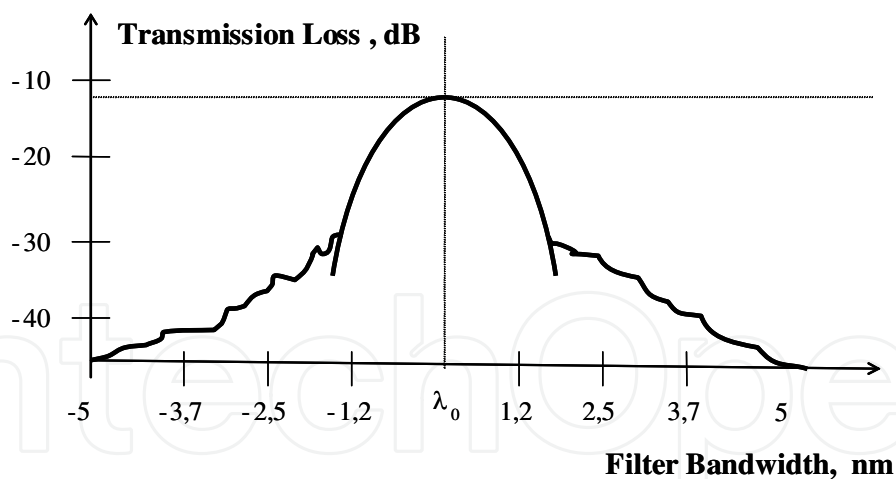


Fig. 7. Holographic filter shape. For wavelengths close to the central value, $\lambda < \lambda_0 \pm 1.5$ nm, the shape is Gaussian and like a Bessel function for wavelengths $\lambda > \lambda_0 \pm 1.5$ nm

n	180	136	94	55
λ_0 (nm)	1431	1471	1511	1551
BW (nm)	1	1	1	1
$\Delta\lambda$ (-3 dB)	1430.5-1431.5	1470.5-1471.5	1510.5-1511.5	1550.5-1551.5
$\Delta\lambda$ (>50 dB)	1421-1441	1461-1481	1501-1521	1541-1561

Table 5. Tunable pass band filter (CWDM)

This feature allows the possibility of a multiple pass band filter in the same optical fiber, but with an increment of losses penalty according to the expression $10 \log C$ (dB), where C is the number of simultaneously tuned channels (Parker et al., 1998). In this case, $C = 4$ and therefore the increment of losses in the device is: $\Delta \text{ losses} = 10 \log 4 = 6$ dB.

4.2 Loss estimation

There are three different sources of loss in this holographic device:

a. SLM losses

An FLC-SLM works as a dynamic full π -binary phase fixed grating hologram with a diffraction efficiency $\eta = 36.5\%$ (4.38 dB) for the first diffractive order ($m = 1$) and a FLC switching angle of 45° .

Another cause of losses is the insertion of the hologram, for a phase SLM, as a result of the light polarization plane and FLC switching angle different to 45° (theoretical optimal angle); at least another 2 dB are lost, assuming a good alignment of the collimated input light and the FLC pixels.

b. Fixed grating losses

The diffraction efficiency for a fixed grating, binary π -phase, is $\eta = 36.5\%$ for the first diffractive order ($m=1$). That means a loss of 4.38 dB.

c. Fiber/lens coupling efficiency

A fiber/lens coupling efficiency of 50% is a good approximation; therefore another 3 dB of losses have to be added (2 dB, with very good alignment).

Losses can be improved using multiple-phase or blazed gratings; in this case the efficiency can reach $\eta \approx 80 - 90\%$ and the losses decrease to 1.5 dB (Ahderom, Raisi et al., 2002).

The estimated total losses of the device are: SLM losses + fixed grating losses + fiber/lens coupling losses = $(4.38+2) + 4.38 + 3 = 13.76$ dB and with loss optimization: $(1.5+2)+1.5+2 = 7$ dB can be obtained.

5. WDM (wavelength division multiplexing) application

We can use this device as a $1 \times M$ demultiplexer, where M is the number of output fibers. For this, a fixed value of n is used and the output fibers are located in certain x positions. Output fibers ($9/125 \mu\text{m}$) must be placed in agreement with the diffracted angles Φ , according to input wavelengths and they have to be separated at least $\Delta x = 125 \mu\text{m}$.

From (5), we can calculate the Δx taking the value of center to center wavelength channel separation, $\Delta\lambda$, into account:

$$x \approx \lambda f \left(\frac{n}{ND} + \frac{1}{d} \right) \Rightarrow \Delta x \approx \Delta\lambda f \left(\frac{n}{ND} + \frac{1}{d} \right) \quad (9)$$

In order to design a compatible device with the frequency grid provided in ITU-T G.694.1/G.694.2 Rec. for CWDM/DWDM systems, a 1×4 demultiplexer ($M = 4$) for DWDM¹ with $\Delta x = 161 \mu\text{m}$ and a 1×8 demultiplexer ($M = 8$) for CWDM with $\Delta x = 321 \mu\text{m}$, can be implemented.

¹ In this case, $\Delta\lambda$'s < 20 nm are not feasible due to the physical dimension of the device (i.e. $\Delta\lambda = 2$ nm and $\Delta x = 161 \mu\text{m} \rightarrow f$, focal distance of the lens, = 25 cm).

Table 6 summarizes the fiber positions in order to demultiplex the wavelengths used in the CWDM/DWDM systems. A CWDM system uses $F_1, F_2, F_3, F_4, F_5, F_6, F_8$ and F_{10} and a DWDM uses F_7, F_8, F_9 , and F_{10} output fibers (see Fig. 6). It is necessary to emphasize that a better performance as demultiplexer could be implemented if only this function is required. For example, we could design a demultiplexer device with channel separation smaller than 50 GHz (Parker, Cohen et al., 1997). However, the novel idea is to design a compatible CWDM/DWDM device able to carry out different functions.

Output fiber	λ (nm) CWDM	λ (nm) DWDM	$x(\mu\text{m})$
F_1	1311		10 535
F_2	1351		10 856
F_3	1391		11 178
F_4	1431		11 499
F_5	1471		11 821
F_6	1511		12 142
F_7		1531	12 303
F_8	1551	1551	12 463
F_9		1571	12 624
F_{10}	1591	1591	12 785

Table 6. CWDM/DWDM demultiplexers ($n = 180$)

6. Wavelength routing application

Maintaining output fibers in the same place as shown in Table 6, if n value (type of hologram) is properly varied, a certain wavelength coming from the input fiber can be routed to any one of the output fibers. As an example, Table 7 highlights the n values for routing $\lambda_0 = 1431\text{nm}$ (CWDM) and $\lambda_0 = 1551$ (DWDM) towards an output fiber; these values have been calculated from (10), considering the variation of n according to Δx :

$$n \approx \left(\frac{x}{\lambda f} - \frac{1}{d} \right) ND \Rightarrow \Delta n \approx \left(\frac{\Delta x}{\lambda f} \right) ND \quad (10)$$

For $\Delta x = 161 \mu\text{m}$, Δn was calculated by using (10) resulting in $\Delta n = 21$ and for $\Delta x = 321 \mu\text{m}$, Δn is 45. Therefore, the device is a $1 \times 8 \lambda$ router in case of CWDM and a $1 \times 4 \lambda$ router for DWDM systems. It is necessary to highlight that the positions of the fibers are compatible with all applications and that the crosstalk resulting from high-order diffraction beams ($m = \pm 2, \pm 3, \dots$) are outside of the locations of the output array fibers ($\Delta\Phi = 4^\circ$), (Horche, 2004).

Output fiber	CWDM n value $\lambda_0 = 1431 \text{ nm}$	DWDM n value $\lambda_0 = 1551 \text{ nm}$
F_1	44	
F_2	89	
F_3	135	
F_4	180	
F_5	225	
F_6	270	
F_7		159
F_8	315	180
F_9		201
F_{10}	360	222

Table 7. CWDM/DWDM routers

7. Basic experimental results

In this section two complementary experiments have been made. The first one is related to diffraction patterns measurements for different bars holograms and the second one to a SLM characterization for holographic filters, demultiplexers and routers use with reference to the devices whose design and characteristics have been described in the previous sections. Due to the unavailability of components in the laboratory with the characteristics previously described, the experimental optical bench is somewhat different from the appropriate one, but, the measurements obtained are in agreement with the calculations.

In order to carry out the measurements, the experimental lab bench showed in Fig. 8 was used; it is in agreement with the structure of Fig. 6, but, in this case, we used a reflective SLM instead of a transmissive one; therefore, it is necessary to include a polarizing beam splitter in order to direct the reflected beam to the lens. Due to the “spatial invariability” of the Fourier transform, it is not necessary to illuminate the entire SLM active surface to reproduce the diffraction pattern; taking this into account we can select, by a diaphragm aperture, the SLM zone where the incident light is focused. The characteristics of a commercial binary phase SLM are shown in Fig. 8(c).

As optical sources, a green He-Ne laser and a tunable Argon laser with $\lambda_g = 528.7 \text{ nm}$ (green) and $\lambda_b = 462.6 \text{ nm}$ (blue) have been used. These wavelengths have been selected because they belong to the visible spectrum and the correct alignment of the system is easier, a critical factor in the experiment. In this case, a detector-array ($6.3 \times 4.7 \text{ mm}$) of a CCD camera is placed at the “focal plane”, as an image sensor, to analyze the results.

A single personal computer, PC, is used to generate the CGHs for the design process described previously, and they are loaded onto the SLM by changing its pixels state; the diffracted patterns were stored in the same PC, where they could be observed and processed. To recalculate the new output fibers position, the distance for the diffraction order (x) is derived from (5) without the fixed grating:

$$x = \lambda \cdot \frac{f}{H} \quad (11)$$

where H , defined in (4), is the hologram spatial period, but now, the maximum value for $n = N/2 = 128$, the size of the pixel, $D = 15 \mu\text{m}$ and the number of pixels in one dimension of the

SLM, $N = 256$, have been taken into account. Fig. 9 summarizes the new fiber positions (F_1 to F_8) with a separation of $\Delta x = 176.23 \mu\text{m}$ between them.

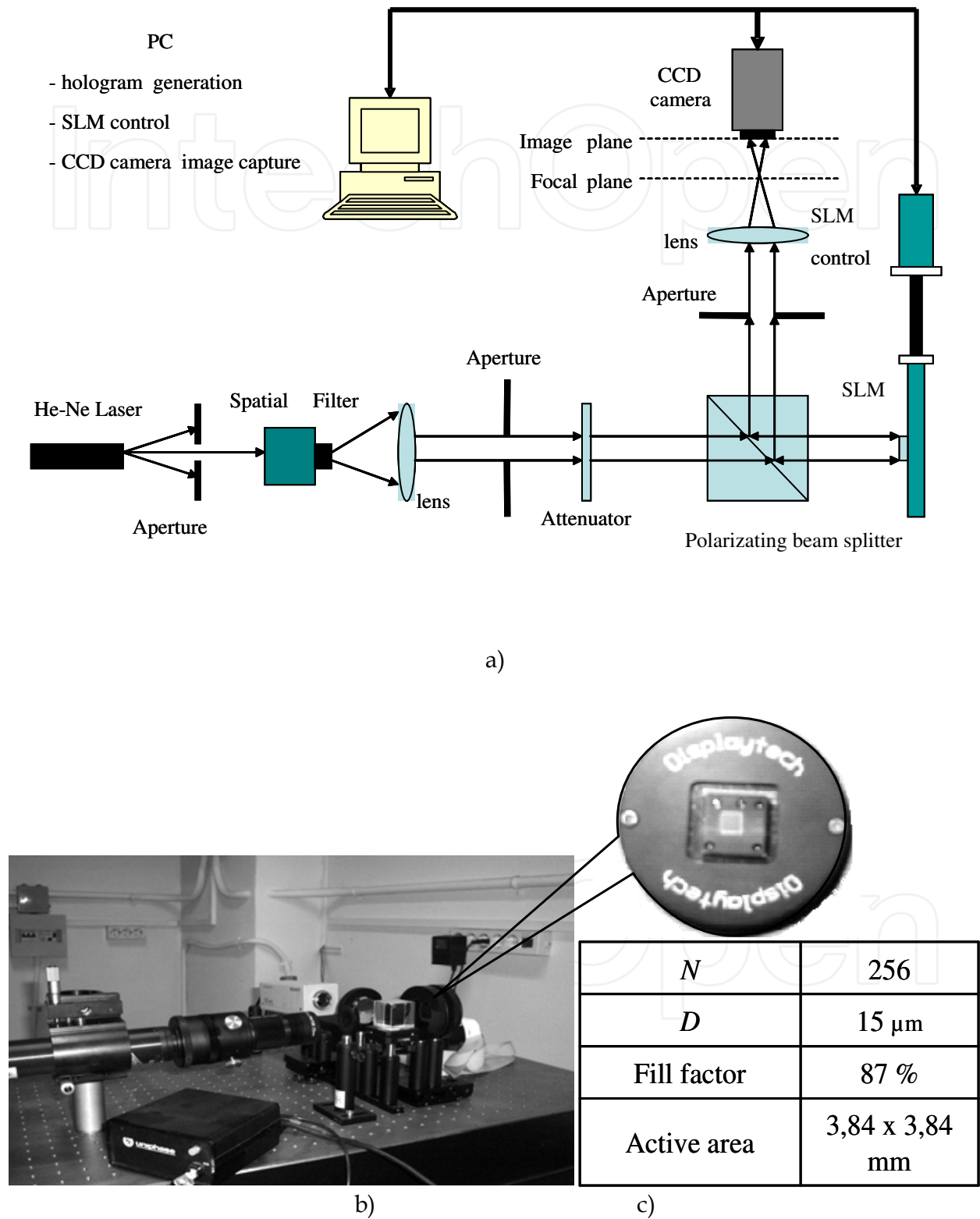


Fig. 8. (a) Optical bench diagram; (b) experimental optical bench and c) binary phase SLM characteristics

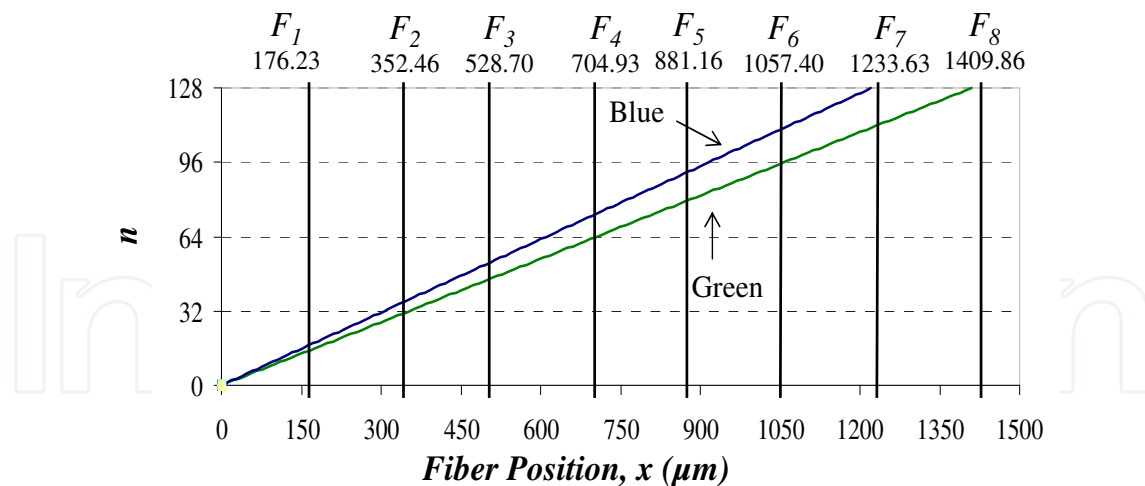


Fig. 9. New output fiber positions for the experimental measurements with two different λ 's: $\lambda_g = 5287$ nm (green) and $\lambda_b = 4626$ nm (blue)

7.1 SLM characterization for wavelength routers

When we implement different holograms, according to n values, in the SLM and an incident light wavelength is illuminating the pixels, different diffracted angles are obtained; by placing an array of fibers at the output, in the focal plane, a λ -router is implemented.

To test the capability of a commercial SLM as a part of a dynamic holographic router, the holographic setup shown in Fig. 8 (a) was implemented; a photo of the experimental optical bench is shown in Fig. 8(b). For this test the optical source was an He-Ne laser at $\lambda = 528.7$ nm (green wavelength) and the lens focal length, 8 cm.

In order to route the green wavelength to the F_4 output fiber, according to Fig. 9, it is necessary to load a CGH-(A) with a spatial period H corresponding to $n = 64$ in the SLM and for routing the same wavelength to the F_8 output fiber, a CGH-(B) with $n = 128$ was calculated and implemented onto the SLM.

7.2 SLM characterization for filters and demultiplexers

Other measurements, to test the capability of a commercial SLM as a part of a dynamic holographic device, have been done with the holographic setup shown in Fig. 8 (Alarcón, 2004). According to Fig. 9, if a CGH black & white bars type hologram with $n = 128$ is loaded onto the programmable SLM, a blue wavelength channel will reach the F_7 output fiber and a green wavelength channel will reach the F_8 output fiber.

The diffracted light spots distance, calculated from (9) without a fixed grating, is:

$$\Delta x \approx \Delta \lambda f \left(\frac{n}{ND} \right) \quad (12)$$

where: $\Delta \lambda = 66.1$ nm; $f = 8$ cm; $n = 128$; $N = 256$ and $D = 15$ μ m.

In Fig.10 light spots captured by CCD camera, from the CGH with $n = 128$ (black and white bars) are shown. In this case the tunable Argon laser with the blue and green colors has been used. The experimental diffracted light spot distances were $x_{blue} = 1233.6$ μ m (F_7) and $x_{green} = 1409.8$ (F_8) μ m, separated by $\Delta x = 176.25$ μ m according to Fig. 9, in good agreement with (12). Therefore, in this way, we can build an optical 1x2 demultiplexer.

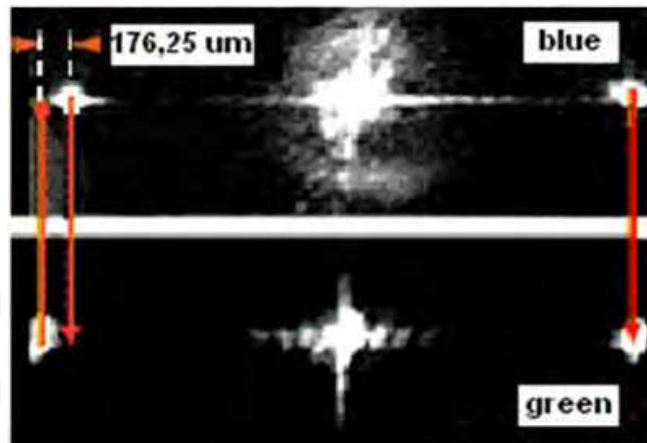


Fig. 10. Diffracted wavelengths with a phase FC-SLM. A tunable Argon laser with $\lambda_g = 528.7$ nm (green) and $\lambda_b = 462,6$ nm (blue) is used. An $\Delta x = 176.25 \mu\text{m}$ (diffracted wavelengths separation) is obtained

The central light spot is due to the zero diffraction order $m = 0$, with the maximum light intensity diffracted ($x = 0$); it can be reduced with a SLM with better performance by impacting on the total insertion losses reduction.

The temporal response of the system was also measured. The SLM optical switching time was estimated to be roughly $250 \mu\text{s}$, as the sum of the electric storage and FLC material response times (Alarcón, 2004). We also noticed a damped response when low-frequency switching is carried out; this is probably due to relaxation of the FLC molecules.

8. Design of equalized holographic ROADMs for application in CWDM metro networks

These type of ROADMs are designed for application in CWDM (Coarse Wavelength Division Multiplexing) networks, where the distance between the different wavelengths allow the use of DML (Direct Modulation Lasers) without cooling, reducing the cost and the tolerances of the network components. Application in METRO networks and its interconnection with some PON (Passive Optical Network), as a part of the access to the subscriber, is reviewed.

Different technologies have been proposed for the implementation of ROADMs (Ma & Kuo, 2003), (Homa & Bala, 2008). Each of them has its own advantages and drawbacks. The main characteristic of holographic ROADMs is the easy way of changing the tuning and power level of the signal at the output fibers by the dynamic implementation of different holograms on the SLM according to the requirements of the network management.

8.1 Holographic ROADM structure

The working principle of the dynamic holographic device is based on the wavelength dispersion produced in a diffraction component (grating, spatial light modulator) as explained in Section 3.

We use for this application a phase reflective spatial light modulator (SLM) and a fixed transmissive diffraction grating to select the corresponding output wavelength from an set of channels in the input, as shown in Fig 11. The active element of the SLM is a Ferroelectric Liquid Crystal (FLC) with a low switching time (less than $50 \mu\text{s}$) that allows a real time

operation. The role of the fixed diffraction grating is to provide more wavelength tuning range and greater total diffraction angle.

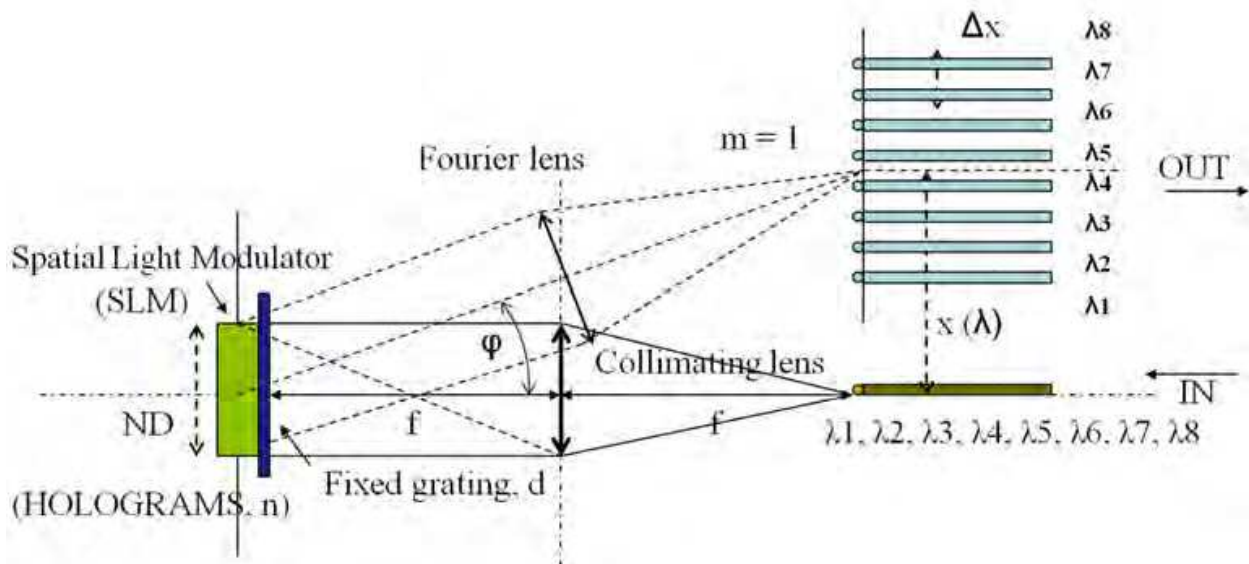


Fig. 11. Reflective holographic router

One of the reasons because we have chosen this type of “2f-folded” implementation, is the reduced size of the device in comparison with the other possible structure, “linear-4f”, where the length of the optical axis is four times the focal distance of the lens used. Its working operation has been described in Section 3.

8.2 Holographic ROADM design

8.2.1 Dynamic wavelength tuning

At the input of the router there are different wavelengths $\lambda_1, \lambda_2, \dots, \lambda_n$ according to some ITU Rec. For the design of this holographic router, these wavelengths are in agreement with the G.694 Rec. for use in CWDM systems. The range of wavelengths is from 1271 nm to 1611 nm with 20 nm as separation between channels; 4, 4+4, 8, 12 and 16 groups of channels are specified distributed along the complete range.

In a holographic router the tuning of this wavelength range is achieved by changing the spatial period of the hologram ND/n , where n is the number of pairs of bars (2-phases) or number of four bars (4-phases), N is the number of pixels and D the size of the SLM pixels. The expression which allows the selection of the output wavelength λ , according to the physical parameters and structure of the device, is (Martin Minguez & Horche, 2007):

$$\lambda \approx \frac{x}{f} \cdot \frac{1}{\left(\frac{n}{ND} + \frac{2}{(M/2) \cdot d} \right)} \quad (13)$$

where x is the distance from the optical axis to the output fiber, f is the focal length of the lens, d is the spatial period of the fixed diffraction grating and M is the number of phases. Fig. 12 shows some tuned wavelengths according to different values of n , for a typical holographic device.

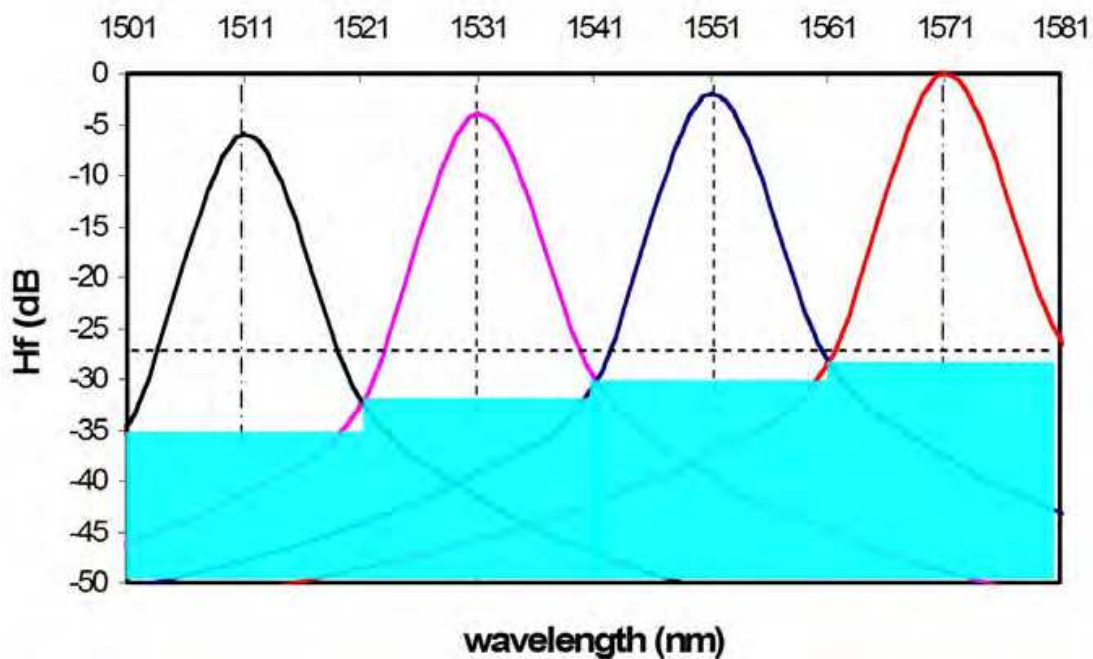


Fig. 12. Four different tuned wavelengths at the output of the holographic router

As we have commented in Section 4.1, for wavelengths close to the central value, the filter response is very similar to the Gauss filter; for wavelengths far from the central value, the filter response is similar to a 3rd order Bessel filter with less out band attenuation. Both of them have a linear phase characteristic, which means a constant group delay. These simulations are in agreement with experimental measurements shown in (Parker et al., 1998).

8.2.2 Holographic device losses

The losses produced in this holographic router, as we have commented before, are due to the following causes:

- *diffraction loss*: the total light diffraction is composed of the transmissive diffraction in the grating (twice) and the reflexive diffraction in the SLM. Using a 4-phases SLM and a grating with 1st order intensity efficiency of about 80%, the total losses are $10 \times \log(3 \times 0.8) \approx 3$ dB.
- *intrinsic SLM loss*: it is due to the liquid crystal (LC) switching angle different from optimal and the coverage of SLM aperture ($1/e^2$ of $ND \times ND$). A typical value is 2 dB.
- *fibres/lens coupling*: by considering 90% efficiency, 1 dB is added.

In total, with an optimized holographic device, a loss about 6 dB has to be taken into account.

8.2.3 Channel power equalization

Power equalization at the all output channels is necessary to compensate the different response of the network components and distances for the used channel wavelengths. To reach it and to compensate for the holographic device losses, a gain component, such as a Semiconductor Optical Amplifier (SOA), has to be employed. The total equalization takes into account the gain-wavelength variation of this amplifier, ΔG_A , whose typical response is drawn in Fig. 13, (the maximum gain, G_A is about 20~25 dB).

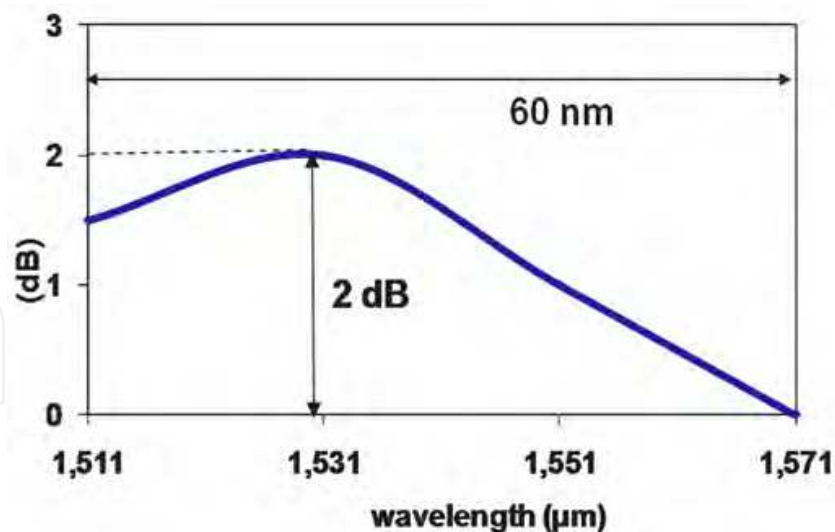


Fig. 13. Incremental gain (ΔG_A) of a typical CWDM SOA

The target is to have at the output fibers a net loss of 0 dB (GT), according to the equation:

$$G_T = G_A - \Delta G_A - 10 \log(\text{number.of.channels}) - L_{HR} - \Delta At = 0 \quad (14)$$

where ΔAt is the total attenuation range for channels to be equalized at the input of the device; L_{HR} is the intrinsic holographic router losses (≈ 6 dB) and the term $\Delta L_{HR} = 10 \times \log(\text{number of channels})$ has taken into account the additional loss due to the mixed holograms utilized for equalizing all the input channels. This point will be explained in detail in the following paragraphs. Fig. 14 shows the structure of an Equalized Holographic ROADM (EH-ROADM) for 4 input channels with full routing of them to the 4 output fibers. A way to obtain at the output fibers tuned wavelengths with different relative attenuation between them is to control the losses due to the SLM aperture, as pointed out in Fig. 15.

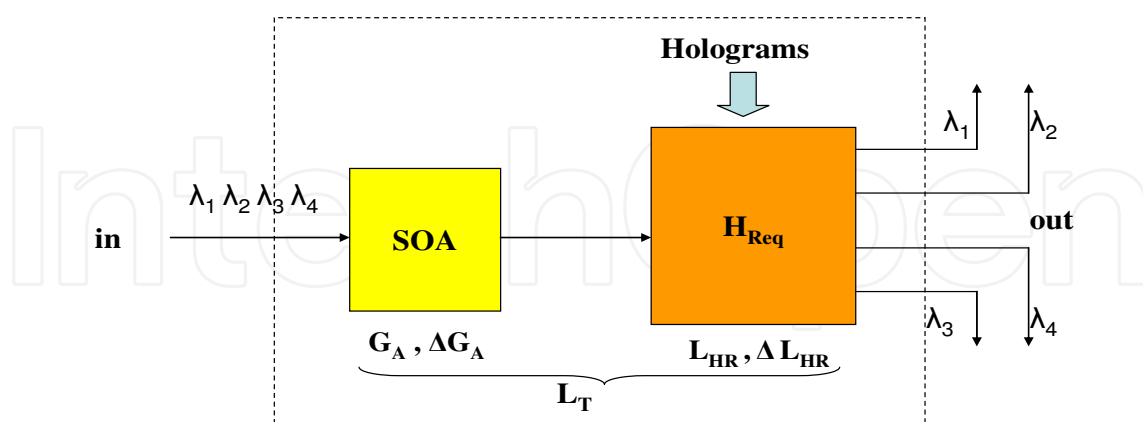


Fig. 14. Equalized Holographic ROADM 1x4

The minimum losses due to the SLM aperture are obtained when the incident light, with a Gaussian distribution, fills the complete surface $ND \times ND$ of the SLM. Therefore, the losses are proportional to the quantity of SLM aperture illuminated by the collimated light coming from the lens, as in Fig. 15. A practical way to reach the former condition is by changing the size of the hologram according to the number of active pixels.

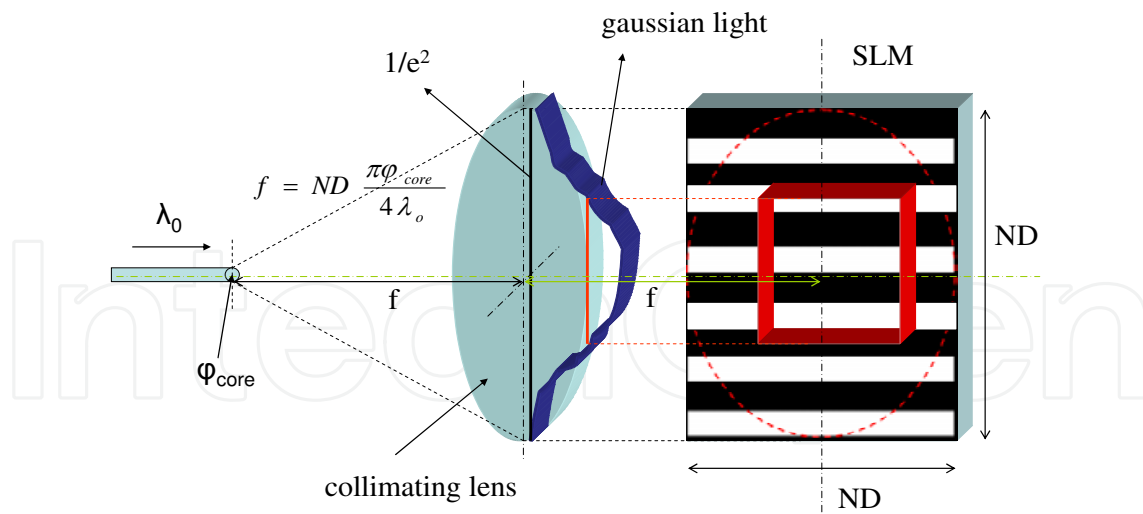


Fig. 15. Losses in the incident light due to different ND x ND hologram apertures

8.2.4 Mixed hologram operation

The EH-ROADM is able to select at the output fibers any combination of wavelengths at the input fiber, from all input wavelengths in just one output fiber to each input wavelength at the corresponding output fiber, including all intermediate cases. This operation mode is done by the selection in the SLM of a mixed hologram composed of all individual holograms corresponding to each input wavelength.

Fig. 16 shows an example for three input wavelengths and its holograms, formed, in this case, by black and white bars (2-phases). For every input wavelength (channel) a hologram is assigned, where n_i (spatial period) produces the pass-band filter for the channel and N_i

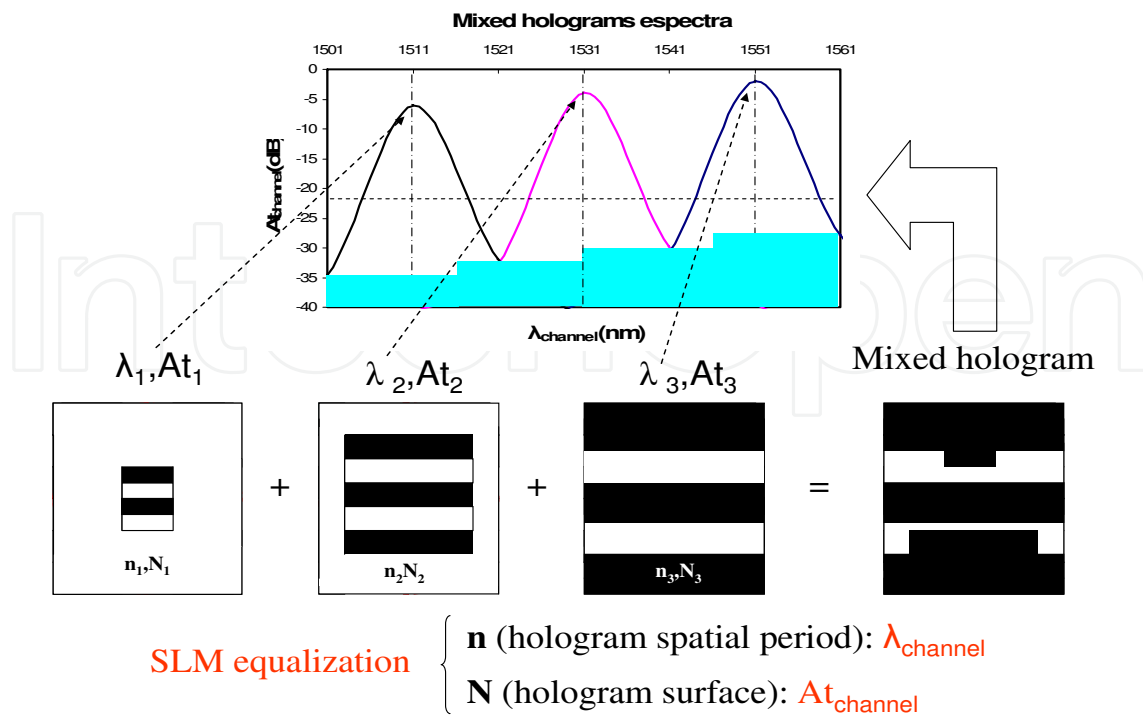


Fig. 16. Mixed holograms operation

takes into account the number of active pixels to reach the correct attenuation, $At_{channel}$, to equalize the output signals. This mixed hologram produces the additional loss in the holographic router, $10 \times \log(\text{number of channels})$. A more fitted equalization can be obtained by monitoring the outputs with a feed-back loop to adjust the size of the holograms according to the wanted output signal level.

8.2.5 Design calculations

Having chosen the SLM, the focal length of the lens, f , to illuminate with collimated light the complete active surface $ND \times ND$ of the SLM (see Fig.15), is related to the number of pixels N and their size D according to expression (8):

$$f = \pi \phi_{core} \frac{ND}{4\lambda_0} \quad (15)$$

where ϕ_{core} is the input fiber core diameter and λ_0 the central wavelength in the operation region. The 3 dB pass-band filter bandwidth of the device, BW , is (Parker et al., 1998)

$$BW \geq \phi_{core} \frac{(M/2) \cdot d}{f} \cdot \left(1 - \frac{\lambda_0^2}{(M/2 \cdot d)^2}\right)^{3/2} \quad (16)$$

if the condition $8D \gg d$ is reached, where d is the fixed grating spatial period. For our calculations, we have a reflective 4-phases SLM with $N = 1024$ and $D = 8 \mu\text{m}$ ($ND = 8.192 \text{ mm}$). Then, the focal distance for the lens is 37.655 mm and the $BW \geq 1.52 \text{ nm}$ (190 GHz), d being $= 6.5 \mu\text{m}$, the spatial period of a 4-phases transmissive diffraction grating and $\phi_{core} = 9 \mu\text{m}$ the core diameter of a singlemode fiber. By changing d we can adjust the BW of the holographic filter.

In the expression (13) the selected wavelength of operation is calculated. The value of n is varied from $n = 0$ (for maximum wavelength) and $n = N/4$ (for minimum wavelength); the central wavelength λ_0 is obtained when $n = N/8$. For the design of a 1x4 router working in the upper band of the CWDM grid, 1471-1611 nm, we take $\lambda_0 = 1541 \text{ nm}$. In this case $\lambda_{min} = 1407 \text{ nm}$ and $\lambda_{max} = 1693 \text{ nm}$; these values cover the entire CWDM upper band. The distance from the optical axis to the output fiber, (see Fig. 11), where the 1st order of the total diffraction is produced, is $x = 9.808 \text{ mm}$ and the total diffraction angle $\varphi \approx 14.6^\circ$.

From ITU G.694 Rec., all CWDM channels are spread $\Delta\lambda = 20 \text{ nm}$ to allow Direct Modulated Lasers (DML) wavelength variation with temperature and filter tolerance; therefore, an $\Delta\lambda = (8-1) \cdot \Delta\lambda = 1611-1471 = 140 \text{ nm}$ range assumes $\Delta X = 1260 \mu\text{m}$, according to the relation:

$$\Delta x \approx \Delta\lambda \cdot f \left(\frac{n}{ND} + \frac{2}{(M/2) \cdot d} \right) \quad (17)$$

This is the maximum interval, at the output plane, where all the output fibers have to be placed. That mean, a separation between fibers of $\Delta x = \Delta X / (8-1) = 1260 / 7 = 180 \mu\text{m}$. Single mode fibers have a cladding diameter of $125 \pm 1 \mu\text{m}$, so, we can reduce this separation to aprox. $130 \mu\text{m}$, if it is needed.

	n_{ij} (holograms)				x_j (μm)
	$\lambda_3 = 1511 \text{ nm}$	$\lambda_4 = 1531 \text{ nm}$	$\lambda_5 = 1551 \text{ nm}$	$\lambda_6 = 1571 \text{ nm}$	
Fibre 3	113	95	78	61	9538
Fibre 4	139	121	103	85	9718
Fibre 5	165	146	128	110	9898
Fibre 6	191	172	153	135	10078
N_i (pixels)	256÷1024	256÷1024	256÷1024	256÷1024	

Table 8. Holograms and active pixels for an EH_ROADM 1x4

In an equalized holographic router, the directing of the input wavelengths to the output fibers is done by the choice of three parameters: n_{ij} for wavelength tuning, N_i for power equalization and Δx_j for placing the output optical fibers. Subscript i is related to the number of input wavelengths and subscript j related with the number of output fibers. Having fixed the separation between fibers, in our case $\Delta x = 180 \mu\text{m}$, we obtain the corresponding value of n_{ij} from (13), according to the input wavelength(s) and output fiber(s) considered. As we are managing different sets of n_{ij} values, all of them have to be different in order to avoid cross-talk between wavelengths on different output fibers.

Table 8 shows the holograms (n_{ij}) and number of active pixels (N_i) for a 4-channels grid according to the ITU G.695 Rec. For instance, in Fig. 11, a mixed hologram 113+95+78+61 addresses the 4 input wavelengths ($\lambda_3 + \lambda_4 + \lambda_5 + \lambda_6$) to the output fibre 3; a mixed hologram 113+121+128+135 addresses λ_3 to fibre 3, λ_4 to fibre 4, λ_5 to fibre 5 and λ_6 to fibre 6. In each case, every λ_i has the corresponding N_i range to assure the power equalization at the output. Table 9 is a summary of the losses in the device (SOA+EH-ROADM) according to the different input channels, whose variation in wavelength is in agreement with Fig. 15. In this case, there is a net gain of 10 dB to compensate for the power variation due to different paths of the input channels along the network. The N_i range, 256÷1024, in Table 8 is to compensate a total of 12 dB of attenuation; with a step of $\Delta N_i = 16$ the ripple at the output is < 0.5 dB.

Intrinsic router loss (dB)	6		L_{HR}
Additional mixed hologram loss (dB)	6		ΔL_{HR}
Max. gain of SOA, G_A (dB)	24		$[10 \times \log(4)]$
Min. gain of SOA, G_A (dB)	22		@ 1531 nm
			@ 1571 nm
λ (nm)	ΔG_A (dB)	Total loss (dB)	
1511	1.5	13.5	
1531	2	14	
1551	1	13	
1571	0	12	
Total min. net gain, G_T (dB)	10		

Table 9. SOA gain, EH_ROADM losses and total net gain

8.2.6 CWDM METRO networks application

The use of tunable holographic devices in Access and Metro networks, like demultiplexers or routers has been studied in different papers (Koonen, 2006), (Martin Minguez & Horche, 2010). In Fig. 17 an application for the equalized holographic ROADM is represented.

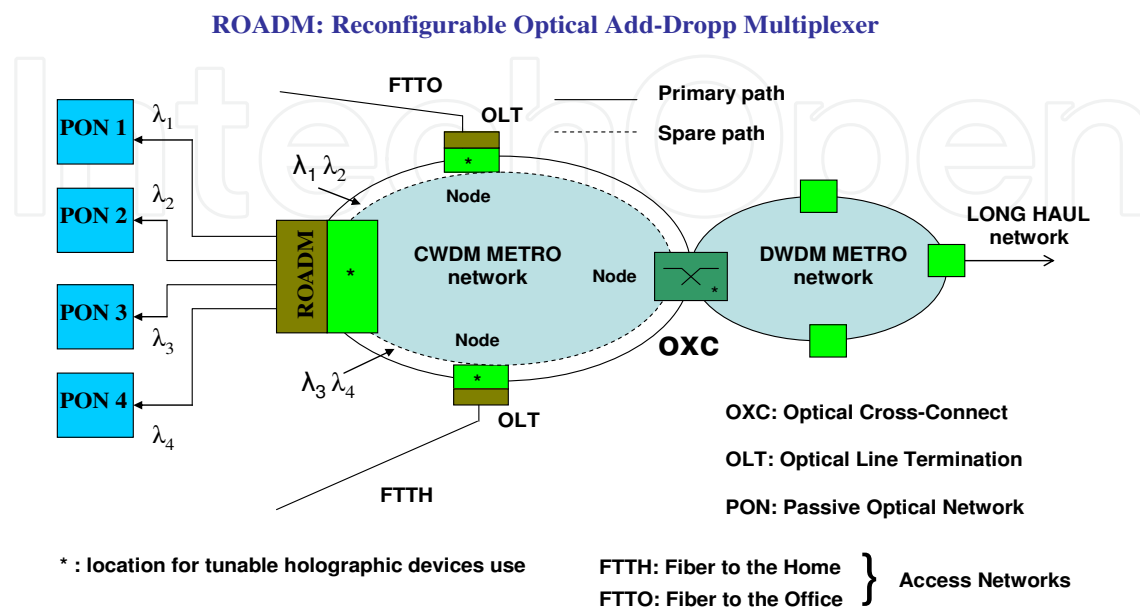


Fig. 17. Application of an EH_ROADM in a CWDM METRO network

A double ring CWDM METRO topology is used to connect this primary access network, through an Optical Line Termination (OLT), with some Fiber to the Office (FTTO) or Fiber to the Home (FTTH) networks with Passive Optical Network (PON) structure; on the other side, a connection to a DWDM METRO network, by an OXC (Optical Cross Connect) with λ conversion, is provided. The target is to address the wavelengths of the double ring network, $\lambda_1, \lambda_2, \lambda_3$ and λ_4 to four different PONs with the possibility of wavelength reallocation.

9. Design of an holographic router with λ conversion and losses compensation

Fig. 18 shows a device composed of a Semiconductor Optical Amplifier (SOA) and a holographic wavelength router. The SOA performs the wavelength conversion by a non linear operation using the Cross Gain Modulation (XGM) method. An incident wavelength, λ_i , modulated by a digital signal is combined with the wavelength λ_{CWj} generated by a tunable laser (CW) into the SOA. At the amplifier output, according to different CW_j wavelengths, λ_{CWj} signals are obtained modulated with the digital signal from the incident λ_i wavelength. These λ_{CWj} signals are also amplified and inverted.

The holographic wavelength router, depending on the input signal, λ_{CWj} , and the generated hologram (n_{ij}) stored in the SLM, addresses this signal to the assigned output. As has been stated, this technology has the drawback of high insertion losses (less than 10 dB, using an optimized device). In order to solve this problem, by combining a SOA with the holographic router, this insertion loss is compensated with the amplifier gain in the saturation zone of operation. A parameter to control in the SOA operation, is related to the amplified spontaneous emission (ASE) because of the impact on the signal distortion.

Fig. 19 shows the simulation of this device, composed of three different blocks: a CW tunable laser, a wavelength conversion semiconductor optical amplifier and a wavelength holographic router. In Fig. 20, the response of the Wavelength Conversion and Routing Holographic Device (WCR-HD) is represented for a 2.5 Gb/s input signal, $\lambda_i = 1540$ nm, which is converted to an output signal, $\lambda_o = 1520$ nm, where the losses of the holographic router are compensated by the gain of the SOA.

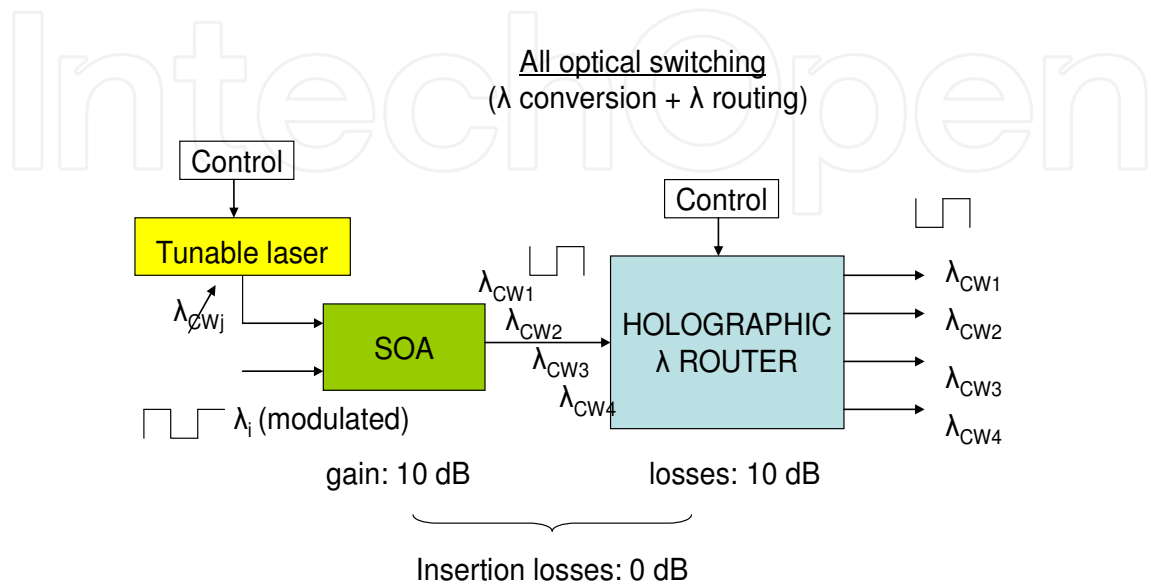


Fig. 18. Device composed of an optical λ converter and a holographic λ router

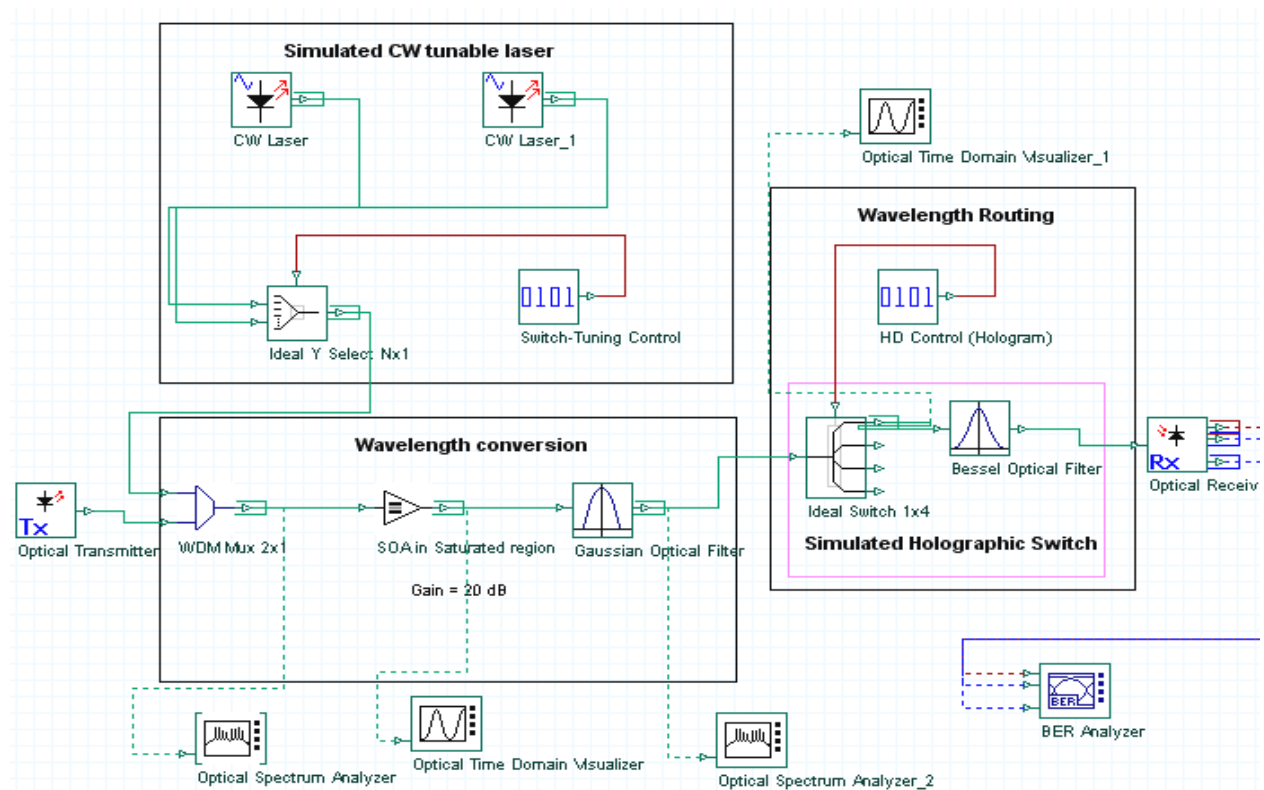


Fig. 19. Wavelength Conversion and Routing Holographic Device (WCR-HD) simulation

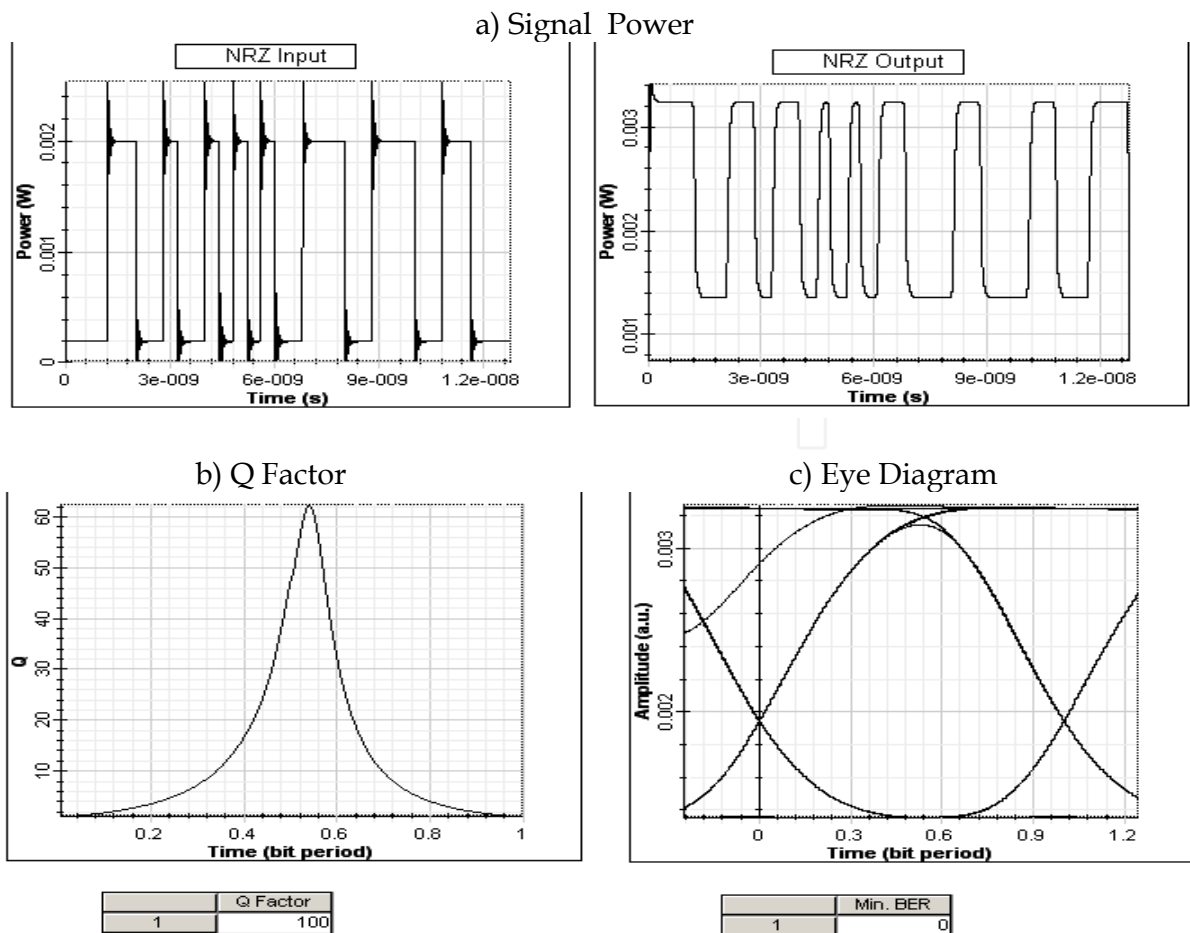


Fig. 20. WCR-HD response for a 2.5 Gbit/s input signal: a) $\lambda_i = 1540$ nm, with wavelength conversion $\lambda_o = 1520$ nm, and losses compensation, b) Q factor ≈ 100 and c) BER ≈ 0 .

10. Conclusion

In this chapter the design of a singular device for use both in CWDM/DWDM systems has been studied. Applications such as, tunable optical filters, demultiplexers and wavelength routers, using holographic SLM technology, have been reviewed taking into account ITU-T G.694.1 and G.694.2 Recs. for central wavelengths allocation.

Application of Computed Generated Hologram design (CGH) to CWDM/DWDM systems has been studied and some comments about this hologram generation technique and its results have been made in order to highlight the phases of the process implementation and the issues related to the diffraction target misalignment and the use of 2-4 phase holograms, etc.

The novel idea in this work is the design of a compatible CWDM/DWDM device able to carry out different multiplexing functions. As we commented before, a better device performance as a tunable filter, demultiplexer or router could be implemented if only one of these functions is required.

The design of equalized holographic ROADMs for applications in CWDM optical networks has been developed. By using a mixed hologram, corresponding to the combination of several input wavelengths, the tuning of a broad range of wavelengths has

been obtained allowing the full routing of several channels from the input fiber to the outputs. As it is possible to change the active pixels in the SLM for each hologram, in order to maintain a fixed output power level, channel equalization has been reached. Intrinsic losses of the device have been optimized using 4-phases holograms whose diffraction efficiency, for the 1st order, is twice that of binary holograms.

Also, the ROADM size has been minimizing by using a "2f-folded" instead of a "linear-4f" for the optical structure. To reduce the total insertion losses of the holographic device a SOA has been added increasing the input power range for equalization. An example of use of these ROADM devices in CWDM Metro and Access Networks (PONs) has been reviewed.

Another example of application is dealing with the design of a holographic router with losses compensation and wavelength conversion, whose main application is in the interconnection nodes of Metro networks. This device uses a SOA (Semiconductor Optical Amplifier), in the non-linear region, to do the wavelength conversion and, in addition, to supply the gain in order to compensate for the intrinsic losses of the holographic router. Other applications in Metro networks like path protection between nodes or switch matrix for ring networks interconnection could be implemented showing the versatility of these devices (Tibuleac & Filer, 2010).

Laboratory experiments testing the capability of a phase FLC-SLM to be used in these devices have been carried out and results show that, for different types of holograms, the possibility of distributing several wavelengths depends on the diffracted angle and, therefore, enabling the building of filters, demultiplexers or wavelength routers.

11. Acknowledgment

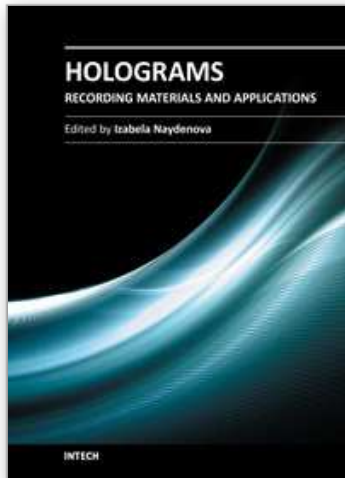
The authors gratefully acknowledge the support of the MICINN (Spain) through project TEC2010-18540 (ROADtoPON).

12. References

- Ahderom S.; Raisi M. et al.. (Jul 2002) "Applications of Liquid Crystal Spatial Light Modulators in Optical Communications", 5th International Conference on High Speed Networks and Multimedia Comm., 3-5, pp 239-242
- Agrawal, G.P. (2002) "Fiber-Optic Communication Systems" (Third Edition), Wiley Interscience
- Alarcón A., (2004) "Dynamic holography applications in SLMs based systems", Master Thesis, ETSITM, Universidad Politécnica de Madrid
- Broomfield S.; Neil M. et al. (1992)"Programmable binary phase-only optical device based on ferroelectric liquid crystal SLM", Electronics Letters, vol. 28 (1), pp. 26-28
- Crossland W. A. et al.. (Dec 2000)"Holographic Optical Switching: The ROSES Demonstrator" IEEE/OSA, J. of Lightwave Tech., vol 18 , no 12, pp 1845-1853
- Dames M.; R. Dowling et al. (1991) "Efficient optical elements to generate intensity weighted spot arrays: design and fabrication", Applied Optics vol. 30, no (19), pp. 2685-2691
- Homa J. & Bala K., (Jul 2008) "ROADM Architectures and Their Enabling WSS Technology" IEEE Communications Magazine, pp 150-153
- Horche P.R.; Alarcón A. et al.. (2004), "Spatial Light Modulator holographic filter for WDM systems", International Union of Radio Science URSI'04

- Kashnow R.A. & Bigelow J.E. (Oct 1973) "Diffraction from a Liquid Crystal Phase Grating", *Applied Optics*, vol. 12, no. 10, pp. 2303-2304
- Koonen T., (May 2006) "Fiber to the Home/Fiber to the Premises: What, Where, and When?" *Proceedings of the IEEE*, Vol. 94, No. 5, pp 911-934
- Ma X, & Kuo G.S., (Nov 2003) "Optical Switching Technology comparison: optical MEMs vs other technologies", *IEEE Optical Communications*, S16-S23
- Martin Minguez A. & Horche P.R, (Jun 2007) "A multipurpose WDM holographic device for filtering, wavelength multiplexing and routing applications", *Photonic Network Communications Journal*, Vol 13, n° 3, pp 313-322
- Martin Minguez A. & Horche P.R., (2010) "Tunable Holographic Components in WDM Optical Networks", *Optical and Quantum Electronics J.*, Volume 42, Issue 1, pp 45-67
- Parker M. C., A.D. Cohen et al., (1997) "Programmable Holographic Elements for WDM", *IEE Colloquium on Optoelectronic Integ. and Switching- Ref N° 1997/372*, 10/1-6
- Parker M. C. et al. (Jul 1998) "Dynamic Digital Holographic Wavelength Filtering", *IEEE/OSA, J. of Lightwave Tech.*, vol. 16, no 7, pp. 1259-1270
- Tibuleac S. & Filer M., (Feb 2010) "Transmission Impairments in DWDM Networks with Reconfigurable Optical Add-Drop Multiplexers", *J. of Lightwave Technology*, vol 28, n° 4, pp 557-568

IntechOpen



Holograms - Recording Materials and Applications

Edited by Dr Izabela Naydenova

ISBN 978-953-307-981-3

Hard cover, 382 pages

Publisher InTech

Published online 09, November, 2011

Published in print edition November, 2011

Holograms - Recording Materials and Applications covers recent advances in the development of a broad range of holographic recording materials including ionic liquids in photopolymerisable materials, azo-dye containing materials, porous glass and polymer composites, amorphous chalcogenide films, Norland optical adhesive as holographic recording material and organic photochromic materials. In depth analysis of collinear holographic data storage and polychromatic reconstruction for volume holographic memory are included. Novel holographic devices, as well as application of holograms in security and signal processing are covered. Each chapter provides a comprehensive introduction to a specific topic, with a survey of developments to date.

How to reference

In order to correctly reference this scholarly work, feel free to copy and paste the following:

Alfredo Martín Mínguez and Paloma R. Horche (2011). Application of Holograms in WDM Components for Optical Fiber Systems, Holograms - Recording Materials and Applications, Dr Izabela Naydenova (Ed.), ISBN: 978-953-307-981-3, InTech, Available from: <http://www.intechopen.com/books/holograms-recording-materials-and-applications/application-of-holograms-in-wdm-components-for-optical-fiber-systems>

INTECH
open science | open minds

InTech Europe

University Campus STeP Ri
Slavka Krautzeka 83/A
51000 Rijeka, Croatia
Phone: +385 (51) 770 447
Fax: +385 (51) 686 166
www.intechopen.com

InTech China

Unit 405, Office Block, Hotel Equatorial Shanghai
No.65, Yan An Road (West), Shanghai, 200040, China
中国上海市延安西路65号上海国际贵都大饭店办公楼405单元
Phone: +86-21-62489820
Fax: +86-21-62489821

© 2011 The Author(s). Licensee IntechOpen. This is an open access article distributed under the terms of the [Creative Commons Attribution 3.0 License](#), which permits unrestricted use, distribution, and reproduction in any medium, provided the original work is properly cited.

IntechOpen

IntechOpen